bioRxiv preprint doi: https://doi.org/10.1101/750877; this version posted August 29, 2019. The copyright holder for this preprint (which was not certified by peer review) is the author/funder. All rights reserved. No reuse allowed without permission.

The effect of APOBEC3B deaminase on double-stranded DNA

Joseph Chapman†, Michael Custance†, Birong Shen*, Anthony V. Furano*

Section on Genomic Structure and Function, Laboratory of Cell and Molecular Biology, National Institute of Diabetes and Digestive and Kidney Diseases, National Institutes of Health, Bethesda, Maryland, 20892, United States

†Contributed equally to this work

*Correspondence should be addressed to A.V.F. (anthonyf@helix.nih.gov) or B.S. (birong.shen@nih.gov)

WITHDRAWN
see manuscript DOI for details

bioRxiv preprint doi: https://doi.org/10.1101/750877; this version posted August 29, 2019. The copyright holder for this preprint (which was not certified by peer review) is the author/funder. All rights reserved. No reuse allowed without permission.

ABSTRACT

Mutations mediated by the APOBEC3 (A3) family of single-strand specific cytosine deaminases can accumulate in various cancers, as strand-coordinated clusters and isolated lesions. A3-mediated mutations also occur during normal development, accounting for ~20% of heritable mutations. A3B is an archetypical member of this family and is thought to contribute to both cancer initiation and progression. A3B has a strong preference for C in a TC context and catalyzes hydrolysis of the primary amine of un-paired C to generate U. Subsequent repair generates a distinctive pattern of C-substitutions, which along with their context signify their A3B origin. Although single-stranded DNA is the preferred A3B substrate, we report here that in some instances A3B can deaminate the C of TC in a double-stranded DNA context *in vitro*. These include C paired to O^6-methylguanine (O^6meG), to an abasic (AP) site, or to a G adjacent to an AP site. AP sites are the most common lesion in DNA, and O^6meG levels increase under alkylating conditions caused by environmental nitrosamines and some chemotherapeutic agents. We also show that elevated expression of A3B can enhance double-stranded breaks induced by the alkylating agent MNNG in mammalian cells, but this effect does not require A3B deaminase activity.

WITHDRAWN
see manuscript DOI for details

INTRODUCTION

Humans encode seven APOBEC3 (A3) single-strand specific cytosine deaminases, which differ in their preference for C in a TC context. These include A3A, A3B, A3C, A3D, A3F, A3G and A3H, although A3G prefers CC[1]. Numerous cancers (including head, neck, bladder, lung, cervical, ovarian, and breast) can accumulate A3-mediated mutations - defined as mutations of C in a TC context to similar amounts of transitions (T) and transversions (A and G)[2-7]. A3 mutations can occur as isolated lesions or in strand-coordinated clusters[8-10]. A3B in particular has been implicated in these mutations and is upregulated in several human cancers[2-4]. Such mutations can also occur in normal cells and account for ~20% of heritable mutations[11].

Single-stranded DNA (ssDNA) generated during transcription, replication, recombination, and repair can result in strand-coordinated clusters of A3B mutations[2-4,11-13]. However, the origin of isolated A3B mutations is less clear. Here we report that compromised hydrogen bonding of C in double-stranded DNA (dsDNA) render it susceptible to A3B deamination *in vitro*. Specifically, C opposite O^6-methylguanine (O^6meG), an abasic (AP) site, or a G adjacent to an AP site, can be deaminated by A3B. We also found that A3B can enhance DNA damage caused by O^6meG *in vivo*, independent of its deaminase activity.

AP sites, which are potentially mutagenic[14], are the most common genetic lesion[15,16] and can result from spontaneous depurination, reactive oxygen species (ROS), and as a consequence of the first step base excision repair (BER) via glycosylase-mediated removal of abnormal or mismatched bases[15,17-22]. U/G and T/G mispairs, due respectively to hydrolytic deamination of C to U or

bioRxiv preprint doi: https://doi.org/10.1101/750877; this version posted August 29, 2019. The copyright holder for this preprint (which was not certified by peer review) is the author/funder. All rights reserved. No reuse allowed without permission.

methyl-C to T, are major BER substrates and contribute to upwards of 10,000 AP sites produced each day, though this number can vary widely between tissues[15,16,22,23].

O^6meG is highly mutagenic and carcinogenic[24,25], and is produced by alkylating agents such as MNNG[26] and those used for chemotherapy[27-29] as well as by naturally occurring nitrosamines[30]. About 1.1-6.7 adducts per 10^7 guanine residues occur in the liver and their frequency in leukocytes is 0.7-4.6 adducts per 10^8 guanine residues[15,31,32]. Nitrosamines occur in processed food, and their production can be enhanced *in vivo* by nitric oxides[33]. O^6meG can be repaired by O^6-methylguanine-DNA methyltransferase (MGMT) via transfer of the O^6-methyl to the MGMT active site cysteine (Cys145), thereby restoring G and inactivating MGMT[34-41]. Persistence of O^6meG can cause DNA damage and double strand breaks (DSBs).

WITHDRAWN
see manuscript DOI for details

RESULTS

In vitro studies on the interaction between A3B and double stranded DNA.

Fig. **1A** shows the basis of the *in vitro* A3B deamination assay. The DNA strand containing the putative A3B-susceptible C is 5' labeled with fluorescein and annealed to its complementary strand (Supplementary Table **S1**). A3B deamination (from HEK293T extract, Supplementary Fig. **S1**, insert) of C produces U, a substrate for uracil-DNA glycosylase (UDG) which generates an AP site labile to NaOH hydrolysis. The ensuing cleaved product is separated from the intact substrate by gel electrophoresis (MATERIALS AND METHODS). Fig. **1B-D** show that C opposite an O^6meG, AP site, or a G adjacent to an AP site (with or without a nick), when in a T<u>C</u> but not A<u>C</u> context, are substrates for HEK293T extracts from cells, which had been transfected with an A3B-HA expression vector. Increasing the amount of A3B-containing extract increases the amount of cleaved product (Supplementary Fig. **S1**). The DNA sequence 5' of the AP site in the oligonucleotide substrate in Fig. **1D** is 50% G+C, making it unlikely that its frank denaturation rendered the C susceptible to deamination.

The requirement for a T<u>C</u> context indicates that deamination of C is due to A3B-HA activity in HEK293T extracts. We verified this by showing that extracts, which contain A3B-HA mutated at positions in or near the active site (based on previous work by Shi et al.[42], Supplementary Table **S2**) eliminated or significantly reduced (A254G or S282A) deaminase activity (Fig. **2**). In addition, we purified the carboxy terminal domain of A3B (A3B-CTD), which contains the deaminase domain and found it capable of deaminating C opposite either O^6meG (Fig. **3A**) or AP sites (Fig. **3B**), although it is less active than the intact enzyme.

In vivo studies on the interaction between A3B and O^6meG-containing DNA.

Effect of A3B expression on MNNG-treated cells.

bioRxiv preprint doi: https://doi.org/10.1101/750877; this version posted August 29, 2019. The copyright holder for this preprint (which was not certified by peer review) is the author/funder. All rights reserved. No reuse allowed without permission.

Previous studies showed that O^{6}meG generated by MNNG (Fig. **4**), can induce γ-H2AX foci (indicates DSBs[26,43-45]). This occurs because O^{6}meG can be read as an A by replicative DNA polymerases thereby generating a T/O^{6}meG mismatch, a substrate for mismatch repair (MMR)[26,46]. Persistence of O^{6}meG in the single-stranded repair template generated during MMR initiates futile cycles of MMR (or BER[47,48]) as O^{6}meG is repeatedly copied into T, resulting in persistent singe-stranded DNA, with eventual fork collapse and DSBs[26]. C paired to O^{6}meG is susceptible to A3B deamination *in vitro*, suggesting that A3B could aggravate the damage by deaminating C to U, creating an MMR or BER substrate which would generate labile AP sites. To test this, we used Hs578T breast cancer cells, which contain low levels of MGMT mRNA relative to other breast cancer cell lines (Supplementary Fig. **S2A**). Thus, direct repair of O^{6}meG lesions would be impaired in these cells, and they exhibited a dose-dependent increase in O^{6}meG content and γ-H2AX lesions with increasing amounts of MNNG (Supplementary Figs. **S2B,C** and **S3**).

To examine the effect of A3B on MNNG-induced γ-H2AX foci we transfected Hs578T cells with both deaminase competent and deaminase deficient A3B expression vectors. Fig. **5A**, lanes 1 and 2, show that Hs578T nuclear extracts contain substantial TC-specific deaminase activity, which is increased approximately two-fold when cells are transfected with a deaminase competent A3B-HA expression vector (Fig. **5A**, lanes 3 and 4). A3B-HA expression enhances the production of γ-H2AX foci at sub saturating amounts (<100 μM) of MNNG in Hs578T cells (Fig. **5B** and Supplementary Fig. **S4**), and it does not affect the viability of MNNG-treated cells (Supplementary Fig. **S6**).

WITHDRAWN
see manuscript DOI for details

However, robust expression of two deaminase minus A3B proteins (A3B-cat, T214D) (Fig. **6A**, insert, lanes 5 and 7) also increased the production of γ-H2AX foci (generated at 25 μM MNNG) and to about the same extent as deaminase competent A3B-HA expression (Fig. **6B**). These results indicate that deaminase activity is dispensable for the effects mediated by A3B in MNNG-treated cells. Deaminase independent activity has been found in other instances of A3 mediated effects[49-54]. We also found that knockdown of endogenous A3B by siRNA did not affect the level of γ-H2AX foci (Supplementary Fig. **S5**). However, this result may not be surprising, given that endogenous levels of A3B in Hs578T cells may be insufficient to generate observable γ-H2AX foci in the presence of MNNG at the fluorescent threshold we set for these experiments (see MATERIALS AND METHODS, and legend to Fig. **5**).

Fate of O^{6}meG/C-containing DNA.

To generate another *in vivo* readout of the effect of A3B on O^{6}meG-containing DNA, we inserted an O^{6}meG/C base pair (in a T<u>C</u>T or G<u>C</u>C context) into a shuttle vector[12] (Fig. **7**). We introduced the shuttle vector constructs into Hs578T cells that had been transfected with an A3B-HA expressing or empty vector (EV) 40 h earlier. After 24 h we isolated the shuttle vectors and generated libraries from the 150 bp flanking the inserted O^{6}meG for paired-end DNA sequencing (Supplementary Table **S3**). If the O^{6}meG-containing strand underwent replication, or survived

bioRxiv preprint doi: https://doi.org/10.1101/750877; this version posted August 29, 2019. The copyright holder for this preprint (which was not certified by peer review) is the author/funder. All rights reserved. No reuse allowed without permission.

repair, O^6meG would have been read as A, subsequently templating a T. Therefore, if this process occurred efficiently, we would have expected as much as 0.5 of the recovered plasmids to have an A at this site. However, the yield of A was less than 0.015 of the recovered products (Fig. **7B** and Supplementary Table **S4**). Thus, most of the O^6meG-containg strand likely suffered strand breakage due to futile rounds of MMR/BER and other processes, and was lost. This result is consistent with and corroborates the induction of γ-H2AX by MNNG *in vivo* (Fig. **5** and **6**). In contrast, the C-containing strand would have not suffered this fate and likely contributed the great bulk of the shuttle vector that we recovered from these cells.

DISCUSSION

A3 deaminases target the N^4 group of single-stranded C, with varying degrees of preference for the C in a TC motif, highest exhibited by A3B. Here, we showed that A3B can also deaminate such C's in dsDNA, including those opposite an O^6meG, an AP site, or a G adjacent to an AP site (Figs. **1B-D**, **2**, and **3**). Several proposed conformational structures and binding energy calculations show that the decreased O^6-G/N^4-C hydrogen bond strength weakens the O^6meG/C base pair compared to a G/C base pair[24,55]. This weakened O^6-G/N^4-C hydrogen bond could expose the N^4-C to A3 deaminases (Fig. **4**), although a significant amount of substrate may not be deaminated due to O^6meG/C wobble base pairing between the N^4-C hydrogen and the N^1-G, ref[55]. Likewise, deamination of C opposite an AP site may occur because the cytosine is free to rotate, thus providing an easier target for A3B (Figs. **1C, 2,** and **3B**). The deamination of C paired to a G adjacent to an AP site (Fig. **1D**) is likely due to the decreased stability of the duplex DNA even though the N^4-C is not exposed[56]. At least 10,000 AP sites in addition to numerous O^6meG adducts occur randomly throughout the genome and could well be a potential source of previously described random, isolated A3B mutations. Thus, our findings supplement those consistent with the proposed mechanisms for strand-coordinated clusters of A3B mutations observed in many human cancers and some non-cancerous tissues[8-10].

The mode of action of MNNG is similar to other chemotherapeutic alkylating agents such as temozolomide and dacarbazine. They are metabolized to a methane diazonium cation (Fig. **4**), which can generate O^6-meG (as well as other adducts)[57,58], leading to futile cycles of MMR and eventually DSBs. As expected, high levels of MGMT have been correlated with poor outcomes for such alkylating agent chemotherapy by repairing these genotoxic lesions[59-65]. As explained in the RESULTS, we would expect that A3 deaminases could enhance the damage induced by MNNG, especially in the low MGMT-expressing Hs578T cell line as the putative O^6meG/C A3B substrate would be spared. As Fig. **5B** showed, A3B did act synergistically with MNNG in in the production of DSBs, but this effect was independent of its deaminase activity (Fig. **6B**).

A3B, like other members of the A3 family, is a single-strand specific DNA binding protein[53,66]. This property is presumably related to the numerous instances of A3 deaminase-independent effects[49-

WITHDRAWN
see manuscript DOI for details

bioRxiv preprint doi: https://doi.org/10.1101/750877; this version posted August 29, 2019. The copyright holder for this preprint (which was not certified by peer review) is the author/funder. All rights reserved. No reuse allowed without permission.

[54]. Thus, our findings that A3B deaminase activity is not required for its aggravation of MNNG-induced DSBs suggest that it does so as a consequence of binding to the single-stranded regions that characterize MNNG-induced damage, perhaps by interfering with or delaying the eventual repair of these lesions.

We also examined the *in vivo* interaction between A3B and O^6meG/C by inserting this base pair in either a TC or GC context on a plasmid shuttle vector capable of replicating in breast cancer cells (Fig. **7A**)[12]. The results in Fig. **7B** and Supplementary Table **S4** indicated that most of the O^6meG-containing strand did not contribute to the shuttle vector recovered in these experiments, likely because it was irretrievably damaged during DNA repair by various means including fruitless rounds of MMR[26,46]. Recovery was worse when the O^6meG was paired to C in a TC context (*i.e.* an A3B context) than in a GC context, a result consistent with the synergistic of A3B and MNNG treatment in the formation of DSBs (Figs. **5** and **6**).

In summary, our biochemical evidence indicates that subtle alterations to DNA structure can have significant impacts on protein-DNA interactions. Future studies could address the possibility that other APOBEC enzymes, or perhaps other proteins known to interact exclusively with ssDNA, behave in a similar manner to A3B when certain DNA lesions or higher order structures are introduced into double stranded DNA.

WITHDRAWN
see manuscript DOI for details

MATERIALS AND METHODS

Chemicals

1-methyl-3-nitro-1-nitrosoguanidine (MNNG) was purchased from TCI America and dissolved in DMSO as a 1 M stock. 3-(4,5-dimethylthiazol-2-yl)-2,5-diphenyltetrazolium bromide (MTT) was purchased from Invitrogen and dissolved in 1X PBS (pH 7.4) as a 5 mg/mL stock.

Mammalian expression vectors

Mammalian expression vectors were purchased from Invitrogen (pcDNA3.1(+)) and the NIH AIDS Reagent Program (phAPOBEC3B-HA). phAPOBEC3B-HA has a pcDNA3 backbone with a 1275 bp insert including KpnI/XhoI sites and the hAPOBEC3B gene linked to 3 carboxy-terminal HA-tags.

Cell culture and transfection

We propagated HEK293T cells in DMEM with 10% FBS at 37°C in 5% CO_2. We transfected cells with PEI complexes of pcDNA3.1(+) or phAPOBEC3B-HA (6 µg per 10 cm dish) using the manufacturer's protocol. Hs578T cells (ATCC®, HTB-126™) were propagated in DMEM with 10% FBS and 0.01 mg/mL insulin at 37°C in 5% CO_2. We transfected pcDNA3.1(+), phAPOBEC3B-HA, or mismatch plasmids (1.5 µg per well in 6-well plate) using Lipofectamine 3000 Reagent (Thermo Fisher Scientific) following the manufacturer's protocol.

bioRxiv preprint doi: https://doi.org/10.1101/750877; this version posted August 29, 2019. The copyright holder for this preprint (which was not certified by peer review) is the author/funder. All rights reserved. No reuse allowed without permission.

Preparation of mammalian cell extracts

Incubation, extraction, and protein quantification were performed as described previously[67-69]. After plasmid transfection, cells were incubated for 48 h at 37°C in 5% CO_2, harvested and lysed using M-PER Mammalian Protein Extraction Reagent (Thermo Scientific, 78501) (with 1X Roche Complete Protease Inhibitor and 100 mM NaCl). The supernatant was collected after a 10-min 16,200xg centrifugation at 4°C and adjusted to 10% glycerol and centrifuged again for 10-min 16,200xg at 4°C. We determined protein concentration with the Pierce BCA Protein Assay Kit (Thermo Fisher Scientific). Western blots were probed with α-HA (Rabbit) antibody, and α-LaminB1 (Rabbit) antibody as a loading control, followed by Rabbit α-HRP incubation and SuperSignal West Pico Chemiluminescent Substrate (Thermo Fisher Scientific).

Isolation of nuclei

We isolated nuclei as previously described[70]. Cells were resuspended in 5 volumes of extraction buffer A (20 mM Tris-HCl pH 7.5, 100 mM EDTA, 2 mM $MgCl_2$), incubated for 2 min at room temperature, followed by 10 min on ice. We adjusted the extract to 1% NP-40, 1 mM PMSF, and 1X Complete Protease Inhibitor (Roche) and incubated the samples for 15 min on ice. We then passed the extracts through a 20-G needle and collected the nuclear pellet with a 10-min 500xg centrifugation at 4°C. We carried out nuclear lysis, protein extraction, and quantification as described above.

WITHDRAWN
see manuscript DOI for details

A3B deaminase mutants

We introduced mutations in phAPOBEC3B-HA using the Q5 Site-Directed Mutagenesis Kit (NEB) following the manufacturer's protocol. Primers (synthesized by IDT) are listed in Supplementary Table **S2** and their annealing temperatures (T_a) were calculated using NEBaseChanger. All constructs were confirmed by DNA sequencing (ACGT, Inc.). We also used the double deaminase mutant A3B-cat (E68A, E255Q)[2,12].

Oligonucleotides

Oligonucleotides (excluding site-directed mutagenesis primers) were synthesized by Midland BioProducts or IDT and are listed in Supplementary Table **S1**. Oligonucleotides used for the *in vitro* deamination assay were annealed in equimolar ratios (100 mM Tris-HCl pH 7.5, 500 mM NaCl), heated at 95°C for 5 min and cooled to room temperature for 4 h. AP sites were generated by treating oligonucleotides containing an internal uracil with UDG (NEB, M0280S) (0.08U/μL reaction) for 30 min at 37°C immediately before use.

Deamination assay

We performed deamination assays as described previously[67-69,71]. Immediately before performing the assay, cell or nuclear extracts were incubated with RNase A (1 μg/ μL) for 15 min at 37°C, 25 μg of which was incubated for 5 h at 37°C in 40-80 μL containing 500 nM oligonucleotide, 10 mM Tris-HCl pH 8.0, 50 mM NaCl, 1 mM DTT, 1 mM EDTA, 2 U UDG (NEB, M0280S), and 1X UDG buffer

bioRxiv preprint doi: https://doi.org/10.1101/750877; this version posted August 29, 2019. The copyright holder for this preprint (which was not certified by peer review) is the author/funder. All rights reserved. No reuse allowed without permission.

(NEB). We adjusted the reactions to 150 mM NaOH and incubated them for 20 min at 37°C, followed by 5 min at 95°C, then immediately chilled on ice. Samples were heated for 5 min at 90°C in 1X Novex TBE-Urea Sample Buffer (Invitrogen), subjected to 12% 7.5 M Urea PAGE, and imaged using the Fujifilm FLA-5100 (FUJIFILM Life Science).

Purification and activity of A3B-CTD from E. coli

A3B-CTD (residues 187-382 of hAPOBEC3B coding sequence with N-terminal methionine and C-terminal His_6 tag (LEHHHHHH) inserted into the NdeI-XhoI site of the pET21 expression vector)[67] was transformed into Rosetta™ (DE3) Competent Cells (Millipore Sigma), spread on LB/agar plates (50 µg/mL carbenicillin, 34 µg/mL chloramphenicol), and incubated overnight at 37°C. Colonies were inoculated in 4 mL LB (50 µg/mL carbenicillin, 34 µg/mL chloramphenicol) and grown at 37°C 250 rpm until the OD_{600} = 0.4-0.6, at which time the cultures were induced with IPTG (0.5 mM) and incubated overnight at 16°C 250 rpm. Cells were harvested, washed with 1X PBS (pH 7.4), resuspended in 650 µL A3B-CTD lysis buffer (50 mM sodium phosphate buffer pH 7.5, 500 mM NaCl, 2 mM 2-mercaptoethanol), sonicated on ice (50% output, 90 seconds). The lysate was centrifuged for 10 min at 16,200xg 4°C and 600 µL of the supernatant was added to a 50 µL slurry of Ni-NTA Agarose (Qiagen) that had been washed three times with 250 µL A3B-CTD lysis buffer without 2-mercaptoethanol and once with 250 µL of A3B-CTD lysis buffer, leaving a 50 µL slurry. After gentle rotation at 4°C for 3.5 h, the slurry was centrifuged at 80xg for 3 min at 4°C. The slurry was subject to two successive 5 min washes (5 min rotation at 4°C) with 350 µL of A3B-CTD lysis buffer with 20 mM and then with 55 mM imidazole. The protein was eluted with 150 µL A3B-CTD lysis buffer containing 350 mM imidazole (30 min rotation at 4°C). The slurry was centrifuged at 80xg for 3 min at 4°C, and the supernatant was dialyzed against 500 mL A3B-CTD storage buffer (25 mM sodium phosphate buffer pH 7.5, 10 mM DTT, 48% glycerol) overnight at 4°C using a D-Tube™ Dialyzer Mini, MWCO 6-8 kDa (Millipore Sigma). The 23 kDa A3B-CTD was verified using Coomassie Blue staining after PAGE (data not shown). Deamination assays were carried out for 5h at 37°C with 10 µL of A3B-CTD and 25 nM oligonucleotides in 10 mM Tris-HCl pH 8.0, 50 mM NaCl, 1 mM DTT, 1 mM EDTA, 1 U UDG (NEB, M0280S), and 1X UDG buffer (NEB). The remainder of the deamination assay was performed as described above.

γ-H2AX staining

Hs578T cells were transfected with pcDNA3.1(+) or phAPOBEC3B-HA, and after 32 h transferred to a Nunc™ LabTek™ II Chamber Slide™ System (Thermo Fisher Scientific). After 16 h, they were incubated with MNNG for 1 h at 37°C in complete media, washed twice with 1X PBS, and incubated again in media for 1 h at 37°C without MNNG (recovery phase). Cells were washed twice in 1X PBS, fixed with 4% formaldehyde (in 1X PBS) for 15 min at 37°C, followed by permeabilization with 0.1% Triton X-100 (in 1X PBS) for 10 min at room temperature, after which cells were blocked with 1% BSA (in 1X PBS) for 30 min at room temperature and incubated overnight at 4°C with Phospho-Histone H2A.X (Ser139) Antibody (Cell Signaling, 2577) in 1% BSA. Cells were blocked again and incubated for 75 min at room temperature with Goat anti-Rabbit IgG (H+L)

WITHDRAWN see manuscript DOI for details

bioRxiv preprint doi: https://doi.org/10.1101/750877; this version posted August 29, 2019. The copyright holder for this preprint (which was not certified by peer review) is the author/funder. All rights reserved. No reuse allowed without permission.

Cross-Absorbed Secondary Antibody, Alexa Fluor 568 (Thermo Fisher Scientific) (in 1% BSA). The chambers were then disassembled, and Prolong™ Diamond Antifade Mountant with DAPI (Thermo Fisher Scientific) was added, and slides were covered with glass coverslips. After incubating overnight, slides were imaged with a Keyence Digital Microscope using 1/15 and 1/12 second exposure time for blue and red channels, respectively. Analysis was performed using Fiji on 10 random fields per sample. Color thresholding for the red channel was set to determine γ-H2AX$^+$ cells (moments, brightness 50, convert image to binary, count cells ≥ 150 pixels). The number of red-stained nuclei was divided by the number of DAPI-stained nuclei and multiplied by 100 to obtain % γ-H2AX$^+$ cells.

Immunocytological assay (ICA) to detect O^{6}meG levels

An ICA was performed as previously described[72]. Hs578T cells were seeded in a 6-well plate, treated with MNNG as described above, and dotted on Superfrost Plus Gold Slides (Thermo Fisher Scientific). Cells were fixed at -20°C in cooled methanol for 30 min, washed with 1X PBS, treated with an alkali/methanol solution (60% 70 mM NaOH/140 mM NaCl, 40% methanol) for 5 min on ice to lyse the cell membranes, and washed with 1X PBS. Slides were placed in a moist chamber for the remainder of the protocol. They were treated with 540 µg/mL Pepsin (Sigma, P6887) (activated with 20 mM HCl immediately prior to use) for 10 min at 37°C. Slides were washed with 1X PBS and treated with 800 µg/mL Proteinase K (Thermo Fisher Scientific, EO0491) for 10 min at 37°C, washed in PBS-glycine (0.2% glycine) for 10 min, blocked in 5% skim milk (in 1X PBS) for 30 min, and stained with 100 µg/mL EM 2-3 monoclonal antibody (Squarix, SQM003.1) (1:300 in 5% BSA) at 4°C overnight. Following washes with PBS-T (0.25% Tween 20) and 1X PBS, cells were stained with Alexa Fluor 568 Goat anti-Mouse IgG (H+L) (Thermo Fisher Scientific, A-11004) (1:400 in 5% BSA) in a dark moist chamber for 75 min. The cells were washed as above and stained with 1 µg/mL DAPI for 30 min and washed in 1X PBS. Immunoselect Antifading Mounting Medium (Squarix), was applied and coverslips were sealed with nail polish and incubated at 4°C overnight. Slides were imaged with a Keyence Digital Microscope using 1/28 and 1/30 second exposure time for blue and red channels, respectively, and 2 fields per sample were analyzed using Fiji. All cells and 10 background readings in each field of view were measured for area, integrated density, and mean gray values. To calculate corrected total cell fluorescence (CTCF) of each cell, the cell area was multiplied by the average mean gray value of the 10 background readings, and the resulting value was subtracted from the cell raw integrated density. The average CTCF for each sample was calculated by averaging CTCF values for all cells from both fields.

MTT assay

We performed an MTT assay[73] to determine cell viability of MNNG treated Hs 578T cells. Metabolically active cells can reduce MTT (yellow) to formazan (purple). 48 h after Hs578T cells were transfected with pcDNA3.1(+) or phAPOBEC3B-HA, they were incubated in a 96-well plate with MNNG for 16 h at 37°C in 5% CO_2, washed with 1X PBS, and treated with 500 µg/mL MTT for

WITHDRAWN
See manuscript DOI for details

bioRxiv preprint doi: https://doi.org/10.1101/750877; this version posted August 29, 2019. The copyright holder for this preprint (which was not certified by peer review) is the author/funder. All rights reserved. No reuse allowed without permission.

4 h at 37°C in 5% CO_2. Media was removed, DMSO was added to resuspend cells, and absorbance was measured at 595 nm using the Bio-Rad Model 680 Microplate Reader.

siRNA knockdown of A3B

We knocked down endogenous A3B in Hs578T cells using 10 nM siRNA (Dharmacon, J-017322-08-0005) and Lipofectamine RNAiMAX Transfection Reagent (Thermo Fisher Scientific) following the manufacturer's protocol. We used scrambled siRNA (Dharmacon, UAGCGACUAAACACAUCAA, siScr) as a negative control.

qRT-PCR

We extracted mRNA from mammalian cells using the PureLink RNA Mini Kit (Ambion Life Technologies) and synthesized cDNA with the SuperScript™ III First-Strand Synthesis System (Thermo Fisher Scientific). We carried out qRT-PCR with TaqMan™ Universal PCR Master Mix, no AmpErase™ UNG (Thermo Fisher Scientific) on a StepOnePlus Real-Time PCR System (Applied Biosystems).

WITHDRAWN
see manuscript DOI for details

In vivo processing of O^6meG/C base pairs

O^6meG/C base pairs were introduced into an SV40-based shuttle vector[74] in both a TC and GC context as previously described[12]. Briefly, 120U Nt.BbvCI (NEB) was used to nick 60 µg of plasmid in the mismatch region of pSP189-FM1 at 2 positions 39 bp apart on the same strand at 37°C overnight. The nicked strand was removed by annealing to a complementary biotinylated oligonucleotide (Supplementary Table **S1**) for 1 h at 37°C, and the resulting duplex was captured on 3 mg streptavidin-coated magnetic beads (Roche, rotation for 2 h at 37°C). After extraction with phenol-chloroform and precipitation with ethanol, 4 µg of the gapped plasmid was annealed to the appropriate 39 nt oligonucleotides (1:100 molar ratio, Supplementary Table **S1**) and ligated overnight with T4 DNA Ligase (NEB). Restoration of a KpnI restriction site present in the gapped region confirmed incorporation of mismatch oligonucleotides. Immediately before transfection into Hs578T cells, 4 µg of plasmid was treated with 1U Klenow Fragment (3' to 5' exo- ,NEB) for 10 min at 37°C to fill any remaining gapped plasmid [12]. The *O^6meG/C* -containing plasmids were transfected into Hs578T cells that had been transfected with an A3B expression vector (phAPOBEC3B-HA) 40 h prior to introduction of the *O^6meG/C* -containing plasmids. After 24 h, cells were harvested, and plasmids were extracted using the Wizard Plus SV Minipreps DNA Purification System (Promega). Plasmids were then treated with 5U DpnI (NEB) for 30 min at 37°C to degrade any non-replicated plasmids, and used as template DNA for NGS sample preparation using Q5 High-Fidelity DNA Polymerase (NEB) (primers shown in Supplementary Table **S3**). The resulting 287 bp PCR products (amplicons) which include the Illumina adapters and the 151 bp of plasmid DNA that flanked the mismatch region were purified using the QIAquick PCR Purification Kit (Qiagen) and quantified with PicoGreen (Thermo Fisher Scientific). Equimolar amounts of pooled amplicons were subjected to paired-end 2x150 deep sequencing (ACGT, Inc.).

bioRxiv preprint doi: https://doi.org/10.1101/750877; this version posted August 29, 2019. The copyright holder for this preprint (which was not certified by peer review) is the author/funder. All rights reserved. No reuse allowed without permission.

ACKNOWLEDGEMENTS

We thank Dr. Judith Levin and Dr. Tiyun Wu (Section on Viral Gene Regulation, NICHD, NIH) for assistance in optimizing the *in vitro* deamination assay, Dr. Charles Jones (LCMB, NIDDK, NIH) for assisting with site-directed mutagenesis, Chang-Hyeock Byeon (Department of Structural Biology, University of Pittsburgh) for help with A3B-CTD purification, and Dr. Jürgen Thomale (Center for Medical Biotechnology, University of Essen) for generous technical support with the ICA. The A3B-CTD expression vector was a generous gift from Dr. In-Ja Byeon and Dr. Angela Gronenborn (Department of Structural Biology, University of Pittsburgh), and the A3B-cat expression vector was constructed in this lab by Dr. Jia Chen[12] (present address, School of Life Science and Technology, ShanghaiTech University).

WITHDRAWN
see manuscript DOI for details

AUTHOR CONTRIBUTIONS

J.C. proposed the idea of C paired to O^6meG as a possible A3B substrate, and the rest of the authors participated in experimental design, data acquisition and interpretation. J.C., M.C., and A.V.F. wrote the manuscript and B.S. helped in the editing and generation of figures.

FUNDING

This work was funded by the Intramural Program of the National Institute of Diabetes and Digestive and Kidney Diseases, NIH.

COMPETEING INTERESTS

No competing financial interests.

REFERENCES

1 Ebrahimi, D., Alinejad-Rokny, H. & Davenport, M. P. Insights into the motif preference of APOBEC3 enzymes. *PLoS One* **9**, e87679, doi:10.1371/journal.pone.0087679 (2014).

2 Burns, M. B. *et al.* APOBEC3B is an enzymatic source of mutation in breast cancer. *Nature* **494**, 366-370, doi:10.1038/nature11881 (2013).

3 Leonard, B. *et al.* APOBEC3B upregulation and genomic mutation patterns in serous ovarian carcinoma. *Cancer Res* **73**, 7222-7231, doi:10.1158/0008-5472.CAN-13-1753 (2013).

4 Roberts, S. A. *et al.* An APOBEC cytidine deaminase mutagenesis pattern is widespread in human cancers. *Nat Genet* **45**, 970-976, doi:10.1038/ng.2702 (2013).

5 Seplyarskiy, V. B. *et al.* APOBEC-induced mutations in human cancers are strongly enriched on the lagging DNA strand during replication. *Genome Res* **26**, 174-182, doi:10.1101/gr.197046.115 (2016).

6 Taylor, B. J. *et al.* DNA deaminases induce break-associated mutation showers with implication of APOBEC3B and 3A in breast cancer kataegis. *Elife* **2**, e00534, doi:10.7554/eLife.00534 (2013).

bioRxiv preprint doi: https://doi.org/10.1101/750877; this version posted August 29, 2019. The copyright holder for this preprint (which was not certified by peer review) is the author/funder. All rights reserved. No reuse allowed without permission.

7 Chan, K. *et al.* An APOBEC3A hypermutation signature is distinguishable from the signature of background mutagenesis by APOBEC3B in human cancers. *Nat Genet* **47**, 1067-1072, doi:10.1038/ng.3378 (2015).

8 Chan, K. & Gordenin, D. A. Clusters of Multiple Mutations: Incidence and Molecular Mechanisms. *Annu Rev Genet* **49**, 243-267, doi:10.1146/annurev-genet-112414-054714 (2015).

9 Supek, F. & Lehner, B. Clustered Mutation Signatures Reveal that Error-Prone DNA Repair Targets Mutations to Active Genes. *Cell* **170**, 534-547 e523, doi:10.1016/j.cell.2017.07.003 (2017).

10 Kazanov, M. D. *et al.* APOBEC-Induced Cancer Mutations Are Uniquely Enriched in Early-Replicating, Gene-Dense, and Active Chromatin Regions. *Cell Rep* **13**, 1103-1109, doi:10.1016/j.celrep.2015.09.077 (2015).

11 Seplyarskiy, V. B., Andrianova, M. A. & Bazykin, G. A. APOBEC3A/B-induced mutagenesis is responsible for 20% of heritable mutations in the TpCpW context. *Genome Res* **27**, 175-184, doi:10.1101/gr.210336.116 (2017).

12 Chen, J., Miller, B. F. & Furano, A. V. Repair of naturally occurring mismatches can induce mutations in flanking DNA. *Elife* **3**, e02001, doi:10.7554/eLife.02001 (2014).

13 Haradhvala, N. J. *et al.* Mutational Strand Asymmetries in Cancer Genomes Reveal Mechanisms of DNA Damage and Repair. *Cell* **164**, 538-549, doi:10.1016/j.cell.2015.12.050 (2016).

14 Jackson, A. L. & Loeb, L. A. The contribution of endogenous sources of DNA damage to the multiple mutations in cancer. *Mutat Res* **477**, 7-21 (2001).

15 De Bont, R. & van Larebeke, N. Endogenous DNA damage in humans: a review of quantitative data. *Mutagenesis* **19**, 169-185 (2004).

16 Lindahl, T. Instability and decay of the primary structure of DNA. *Nature* **362**, 709-715, doi:10.1038/362709a0 (1993).

17 Amosova, O., Coulter, R. & Fresco, J. R. Self-catalyzed site-specific depurination of guanine residues within gene sequences. *Proc Natl Acad Sci U S A* **103**, 4392-4397, doi:10.1073/pnas.0508499103 (2006).

18 Amosova, O., Kumar, V., Deutsch, A. & Fresco, J. R. Self-catalyzed site-specific depurination of G residues mediated by cruciform extrusion in closed circular DNA plasmids. *J Biol Chem* **286**, 36322-36330, doi:10.1074/jbc.M111.272112 (2011).

19 Amosova, O., Smith, A. & Fresco, J. R. The consensus sequence for self-catalyzed site-specific G residue depurination in DNA. *J Biol Chem* **286**, 36316-36321, doi:10.1074/jbc.M111.272047 (2011).

20 An, R. *et al.* Non-enzymatic depurination of nucleic acids: factors and mechanisms. *PLoS One* **9**, e115950, doi:10.1371/journal.pone.0115950 (2014).

21 Fresco, J. R. & Amosova, O. Site-Specific Self-Catalyzed DNA Depurination: A Biological Mechanism That Leads to Mutations and Creates Sequence Diversity. *Annu Rev Biochem* **86**, 461-484, doi:10.1146/annurev-biochem-070611-095951 (2017).

22 Nakamura, J. & Swenberg, J. A. Endogenous apurinic/apyrimidinic sites in genomic DNA of mammalian tissues. *Cancer Res* **59**, 2522-2526 (1999).

23 Atamna, H., Cheung, I. & Ames, B. N. A method for detecting abasic sites in living cells: age-dependent changes in base excision repair. *Proc Natl Acad Sci U S A* **97**, 686-691 (2000).

WITHDRAWN
See manuscript DOI for details

bioRxiv preprint doi: https://doi.org/10.1101/750877; this version posted August 29, 2019. The copyright holder for this preprint (which was not certified by peer review) is the author/funder. All rights reserved. No reuse allowed without permission.

24 Jena, N. R. & Bansal, M. Mutagenicity associated with O6-methylguanine-DNA damage and mechanism of nucleotide flipping by AGT during repair. *Phys Biol* **8**, 046007, doi:10.1088/1478-3975/8/4/046007 (2011).

25 Abbott, P. J. & Saffhill, R. DNA synthesis with methylated poly(dC-dG) templates. Evidence for a competitive nature to miscoding by O(6)-methylguanine. *Biochim Biophys Acta* **562**, 51-61 (1979).

26 Noonan, E. M., Shah, D., Yaffe, M. B., Lauffenburger, D. A. & Samson, L. D. O6-Methylguanine DNA lesions induce an intra-S-phase arrest from which cells exit into apoptosis governed by early and late multi-pathway signaling network activation. *Integr Biol (Camb)* **4**, 1237-1255, doi:10.1039/c2ib20091k (2012).

27 Fahrer, J. & Kaina, B. O6-methylguanine-DNA methyltransferase in the defense against N-nitroso compounds and colorectal cancer. *Carcinogenesis* **34**, 2435-2442, doi:10.1093/carcin/bgt275 (2013).

28 Povey, A. C. DNA adducts: endogenous and induced. *Toxicol Pathol* **28**, 405-414, doi:10.1177/019262330002800308 (2000).

29 Fu, D., Calvo, J. A. & Samson, L. D. Balancing repair and tolerance of DNA damage caused by alkylating agents. *Nat Rev Cancer* **12**, 104-120, doi:10.1038/nrc3185 (2012).

30 Reh, B. D. *et al.* O(6)-methylguanine DNA adducts associated with occupational nitrosamine exposure. *Carcinogenesis* **21**, 29-33 (2000).

31 Kang, H., Konishi, C., Kuroki, T. & Huh, N. Detection of O6-methylguanine, O4-methylthymine and O4-ethylthymine in human liver and peripheral blood leukocyte DNA. *Carcinogenesis* **16**, 1277-1280 (1995).

32 Kang, H. I. *et al.* Highly sensitive, specific detection of O6-methylguanine, O4-methylthymine, and O4-ethylthymine by the combination of high-performance liquid chromatography prefractionation, 32P postlabeling, and immunoprecipitation. *Cancer Res* **52**, 5307-5312 (1992).

33 Winter, J. W. *et al.* N-nitrosamine generation from ingested nitrate via nitric oxide in subjects with and without gastroesophageal reflux. *Gastroenterology* **133**, 164-174, doi:10.1053/j.gastro.2007.04.047 (2007).

34 Eker, A. P., Quayle, C., Chaves, I. & van der Horst, G. T. DNA repair in mammalian cells: Direct DNA damage reversal: elegant solutions for nasty problems. *Cell Mol Life Sci* **66**, 968-980, doi:10.1007/s00018-009-8735-0 (2009).

35 Fan, C. H. *et al.* O6-methylguanine DNA methyltransferase as a promising target for the treatment of temozolomide-resistant gliomas. *Cell Death Dis* **4**, e876, doi:10.1038/cddis.2013.388 (2013).

36 Shukla, P. K. & Mishra, P. C. Repair of O6-methylguanine to guanine by cysteine in the absence and presence of histidine and by cysteine thiolate anion: a quantum chemical study. *Phys Chem Chem Phys* **11**, 8191-8202, doi:10.1039/b908295f (2009).

37 Tiwari, S. & Mishra, P. C. A quantum chemical study of repair of O6-methylguanine to guanine by tyrosine: evaluation of the winged helix-turn-helix model. *J Mol Model* **15**, 1407-1415, doi:10.1007/s00894-009-0499-9 (2009).

38 Mishina, Y., Duguid, E. M. & He, C. Direct reversal of DNA alkylation damage. *Chem Rev* **106**, 215-232, doi:10.1021/cr0404702 (2006).

39 Mitra, S. MGMT: a personal perspective. *DNA Repair (Amst)* **6**, 1064-1070, doi:10.1016/j.dnarep.2007.03.007 (2007).

WITHDRAWN
see manuscript DOI for details

bioRxiv preprint doi: https://doi.org/10.1101/750877; this version posted August 29, 2019. The copyright holder for this preprint (which was not certified by peer review) is the author/funder. All rights reserved. No reuse allowed without permission.

40 Tubbs, J. L., Pegg, A. E. & Tainer, J. A. DNA binding, nucleotide flipping, and the helix-turn-helix motif in base repair by O6-alkylguanine-DNA alkyltransferase and its implications for cancer chemotherapy. *DNA Repair (Amst)* **6**, 1100-1115, doi:10.1016/j.dnarep.2007.03.011 (2007).

41 Pegg, A. E. Repair of O(6)-alkylguanine by alkyltransferases. *Mutat Res* **462**, 83-100 (2000).

42 Shi, K. *et al.* Structural basis for targeted DNA cytosine deamination and mutagenesis by APOBEC3A and APOBEC3B. *Nat Struct Mol Biol* **24**, 131-139, doi:10.1038/nsmb.3344 (2017).

43 Banath, J. P., Klokov, D., MacPhail, S. H., Banuelos, C. A. & Olive, P. L. Residual gammaH2AX foci as an indication of lethal DNA lesions. *BMC Cancer* **10**, 4, doi:10.1186/1471-2407-10-4 (2010).

44 Staszewski, O., Nikolova, T. & Kaina, B. Kinetics of gamma-H2AX focus formation upon treatment of cells with UV light and alkylating agents. *Environ Mol Mutagen* **49**, 734-740, doi:10.1002/em.20430 (2008).

45 Kinner, A., Wu, W., Staudt, C. & Iliakis, G. Gamma-H2AX in recognition and signaling of DNA double-strand breaks in the context of chromatin. *Nucleic Acids Res* **36**, 5678-5694, doi:10.1093/nar/gkn550 (2008).

46 Singh, J., Su, L. & Snow, E. T. Replication across O6-methylguanine by human DNA polymerase beta in vitro. Insights into the futile cytotoxic repair and mutagenesis of O6-methylguanine. *J Biol Chem* **271**, 28391-28398 (1996).

47 Kim, Y. J. & Wilson, D. M., 3rd. Overview of base excision repair biochemistry. *Curr Mol Pharmacol* **5**, 3-13 (2012).

48 Beard, W. A. & Wilson, S. H. Structure and mechanism of DNA polymerase Beta. *Chem Rev* **106**, 361-382, doi:10.1021/cr0404904 (2006).

49 Matsumoto, T. *et al.* Protein kinase A inhibits tumor mutator APOBEC3B through phosphorylation. *Scientific Reports* **9**, 8307, doi:10.1038/s41598-019-44407-9 (2019).

50 Ma, W. *et al.* APOBEC3B promotes hepatocarcinogenesis and metastasis through novel deaminase-independent activity. *Mol Carcinog* **58**, 643-653, doi:10.1002/mc.22956 (2019).

51 Stenglein, M. D. & Harris, R. S. APOBEC3B and APOBEC3F inhibit L1 retrotransposition by a DNA deamination-independent mechanism. *J Biol Chem* **281**, 16837-16841, doi:10.1074/jbc.M602367200 (2006).

52 Iwatani, Y. *et al.* Deaminase-independent inhibition of HIV-1 reverse transcription by APOBEC3G. *Nucleic Acids Res* **35**, 7096-7108, doi:10.1093/nar/gkm750 (2007).

53 Chaurasiya, K. R. *et al.* Oligomerization transforms human APOBEC3G from an efficient enzyme to a slowly dissociating nucleic acid-binding protein. *Nat Chem* **6**, 28-33, doi:10.1038/nchem.1795 (2014).

54 Bogerd, H. P., Wiegand, H. L., Doehle, B. P., Lueders, K. K. & Cullen, B. R. APOBEC3A and APOBEC3B are potent inhibitors of LTR-retrotransposon function in human cells. *Nucleic Acids Res.* **34**, 89-95 (2006).

55 Warren, J. J., Forsberg, L. J. & Beese, L. S. The structural basis for the mutagenicity of O(6)-methyl-guanine lesions. *Proc Natl Acad Sci U S A* **103**, 19701-19706, doi:10.1073/pnas.0609580103 (2006).

56 Vesnaver, G., Chang, C. N., Eisenberg, M., Grollman, A. P. & Breslauer, K. J. Influence of abasic and anucleosidic sites on the stability, conformation, and melting behavior of a DNA duplex: correlations of thermodynamic and structural data. *Proc Natl Acad Sci U S A* **86**, 3614-3618 (1989).

WITHDRAWN
see manuscript DOI for details

bioRxiv preprint doi: https://doi.org/10.1101/750877; this version posted August 29, 2019. The copyright holder for this preprint (which was not certified by peer review) is the author/funder. All rights reserved. No reuse allowed without permission.

57 Zhang, J., Stevens, M. F. & Bradshaw, T. D. Temozolomide: mechanisms of action, repair and resistance. *Curr Mol Pharmacol* **5**, 102-114 (2012).

58 Kim, K.-W., Roh, J. K., Wee, H.-J. & Kim, C. in *Cancer Drug Discovery: Science and History* 71-94 (Springer Netherlands, 2016).

59 Kitange, G. J. *et al.* Induction of MGMT expression is associated with temozolomide resistance in glioblastoma xenografts. *Neuro Oncol* **11**, 281-291, doi:10.1215/15228517-2008-090 (2009).

60 Kitange, G. J. *et al.* Inhibition of histone deacetylation potentiates the evolution of acquired temozolomide resistance linked to MGMT upregulation in glioblastoma xenografts. *Clin Cancer Res* **18**, 4070-4079, doi:10.1158/1078-0432.CCR-12-0560 (2012).

61 Kreth, S. *et al.* O-methylguanine-DNA methyltransferase (MGMT) mRNA expression predicts outcome in malignant glioma independent of MGMT promoter methylation. *PLoS One* **6**, e17156, doi:10.1371/journal.pone.0017156 (2011).

62 Melguizo, C. *et al.* MGMT promoter methylation status and MGMT and CD133 immunohistochemical expression as prognostic markers in glioblastoma patients treated with temozolomide plus radiotherapy. *J Transl Med* **10**, 250, doi:10.1186/1479-5876-10-250 (2012).

63 Perazzoli, G. *et al.* Temozolomide Resistance in Glioblastoma Cell Lines: Implication of MGMT, MMR, P-Glycoprotein and CD133 Expression. *PLoS One* **10**, e0140131, doi:10.1371/journal.pone.0140131 (2015).

64 Qiu, Z. K. *et al.* Enhanced MGMT expression contributes to temozolomide resistance in glioma stem-like cells. *Chin J Cancer* **33**, 115-122, doi:10.5732/cjc.012.10236 (2014).

65 Kewitz, S., Stiefel, M., Kramm, C. M. & Staege, M. S. Impact of O6-methylguanine-DNA methyltransferase (MGMT) promoter methylation and MGMT expression on dacarbazine resistance of Hodgkin's lymphoma cells. *Leuk Res* **38**, 138-143, doi:10.1016/j.leukres.2013.11.001 (2014).

66 Salter, J. D., Bennett, R. P. & Smith, H. C. The APOBEC Protein Family: United by Structure, Divergent in Function. *Trends Biochem Sci* **41**, 578-594, doi:10.1016/j.tibs.2016.05.001 (2016).

67 Byeon, I. J. *et al.* Nuclear Magnetic Resonance Structure of the APOBEC3B Catalytic Domain: Structural Basis for Substrate Binding and DNA Deaminase Activity. *Biochemistry* **55**, 2944-2959, doi:10.1021/acs.biochem.6b00382 (2016).

68 Mitra, M. *et al.* Structural determinants of human APOBEC3A enzymatic and nucleic acid binding properties. *Nucleic Acids Res* **42**, 1095-1110, doi:10.1093/nar/gkt945 (2014).

69 Mitra, M. *et al.* Sequence and structural determinants of human APOBEC3H deaminase and anti-HIV-1 activities. *Retrovirology* **12**, 3, doi:10.1186/s12977-014-0130-8 (2015).

70 Rosner, M., Schipany, K. & Hengstschlager, M. Merging high-quality biochemical fractionation with a refined flow cytometry approach to monitor nucleocytoplasmic protein expression throughout the unperturbed mammalian cell cycle. *Nat Protoc* **8**, 602-626, doi:10.1038/nprot.2013.011 (2013).

71 Iwatani, Y., Takeuchi, H., Strebel, K. & Levin, J. G. Biochemical activities of highly purified, catalytically active human APOBEC3G: correlation with antiviral effect. *J Virol* **80**, 5992-6002, doi:10.1128/JVI.02680-05 (2006).

72 Melnikova, M. & Thomale, J. Visualization and Quantitative Measurement of Drug-Induced Platinum Adducts in the Nuclear DNA of Individual Cells by an Immuno-Cytological Assay. *Methods Mol Biol* **1655**, 351-358, doi:10.1007/978-1-4939-7234-0_24 (2018).

WITHDRAWN
See manuscript DOI for details

bioRxiv preprint doi: https://doi.org/10.1101/750877; this version posted August 29, 2019. The copyright holder for this preprint (which was not certified by peer review) is the author/funder. All rights reserved. No reuse allowed without permission.

73 van Meerloo, J., Kaspers, G. J. & Cloos, J. Cell sensitivity assays: the MTT assay. *Methods Mol Biol* **731**, 237-245, doi:10.1007/978-1-61779-080-5_20 (2011).

74 Seidman, M. M., Dixon, K., Razzaque, A., Zagursky, R. J. & Berman, M. L. A shuttle vector plasmid for studying carcinogen-induced point mutations in mammalian cells. *Gene* **38**, 233-237 (1985).

WITHDRAWN
see manuscript DOI for details

bioRxiv preprint doi: https://doi.org/10.1101/750877; this version posted August 29, 2019. The copyright holder for this preprint (which was not certified by peer review) is the author/funder. All rights reserved. No reuse allowed without permission.

FIGURES AND FIGURE LEGENDS

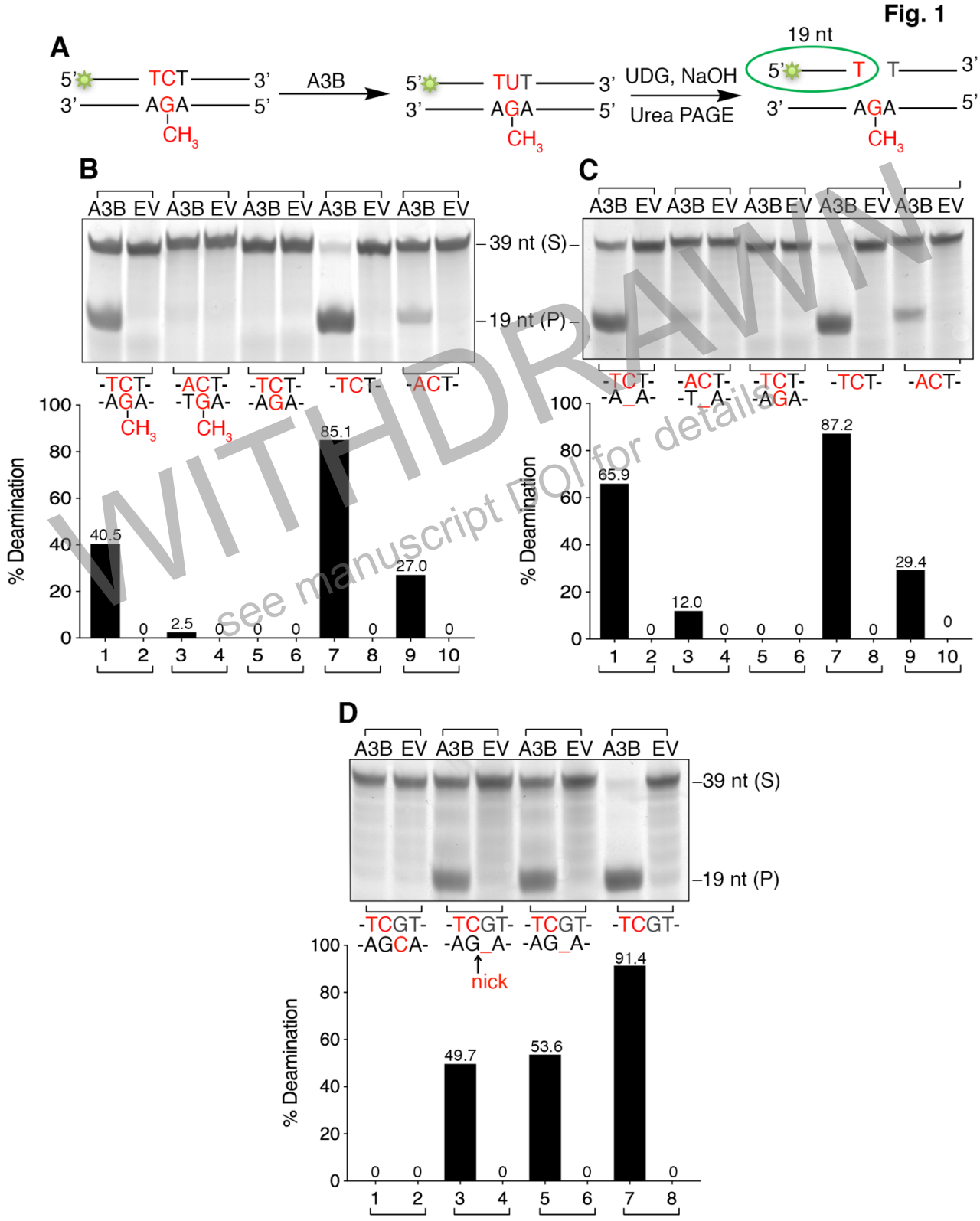

WITHDRAWN
see manuscript DOI for details

bioRxiv preprint doi: https://doi.org/10.1101/750877; this version posted August 29, 2019. The copyright holder for this preprint (which was not certified by peer review) is the author/funder. All rights reserved. No reuse allowed without permission.

Fig. 1*: Cytosines (in a TC context) opposite O⁶meG, AP, or G adjacent to AP sites are A3B substrates in vitro*. (A) Diagram of the *in vitro* deamination assay. (B, C, D) *in vitro* deamination of O⁶meG/C, AP/C, and G/C (adjacent to an AP site with or without a nick). TC-containing ssDNA serves as a positive control, and AC-containing ssDNA and TC-containing dsDNA serve as negative controls. Bar graphs show the amount of cleaved product relative to the amount of starting substrate. A3B, HEK293T whole cell extract containing A3B-HA; EV, HEK293T whole cell extract that had been transfected with an empty vector. S, substrate; P, cleaved product.

WITHDRAWN
see manuscript DOI for details

bioRxiv preprint doi: https://doi.org/10.1101/750877; this version posted August 29, 2019. The copyright holder for this preprint (which was not certified by peer review) is the author/funder. All rights reserved. No reuse allowed without permission.

WITHDRAWN
see manuscript DOI for details

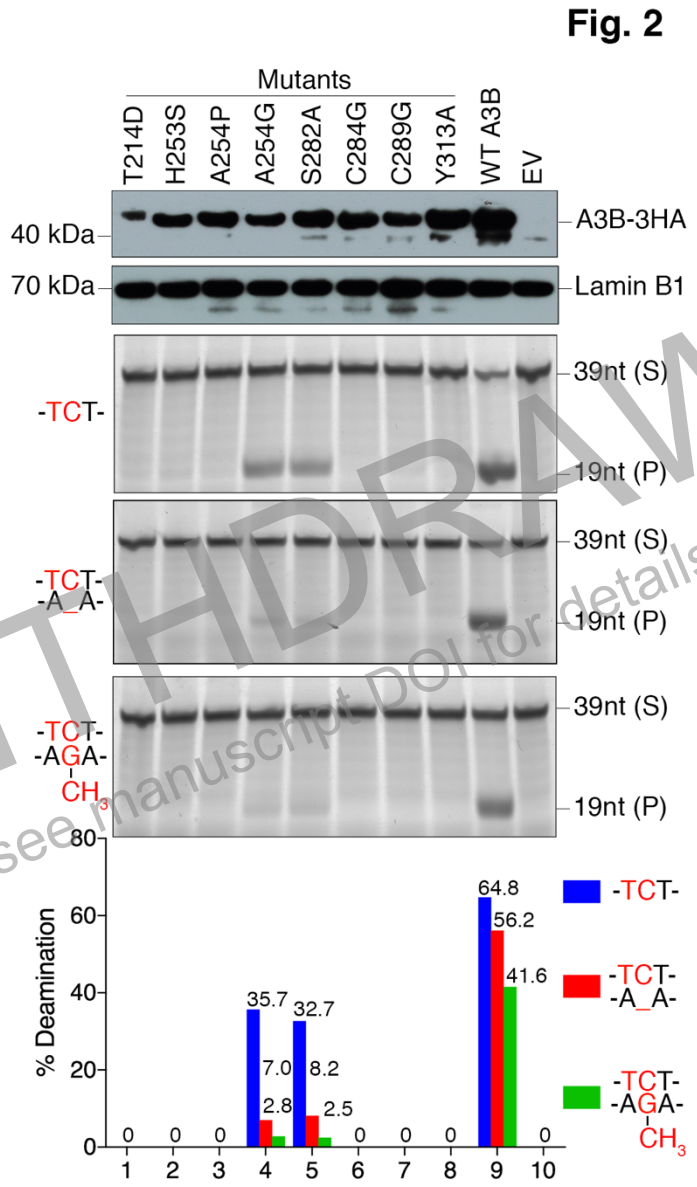

Fig. 2*: Deaminase activity of A3B mutant proteins*. Western blots of HEK293T nuclear extracts from cells transfected with expression vectors containing various mutant A3B-HA proteins probed with α-HA, or α-LaminB1 as a loading control (top 2 panels). *in vitro* deamination of A3B mutant proteins in HEK293T nuclear extract for different 39 bp oligonucleotides (bottom 3 panels). The bar graphs show the amount of cleaved product relative to the amount of starting substrate. S, substrate; P, cleaved product.

bioRxiv preprint doi: https://doi.org/10.1101/750877; this version posted August 29, 2019. The copyright holder for this preprint (which was not certified by peer review) is the author/funder. All rights reserved. No reuse allowed without permission.

Fig. 3

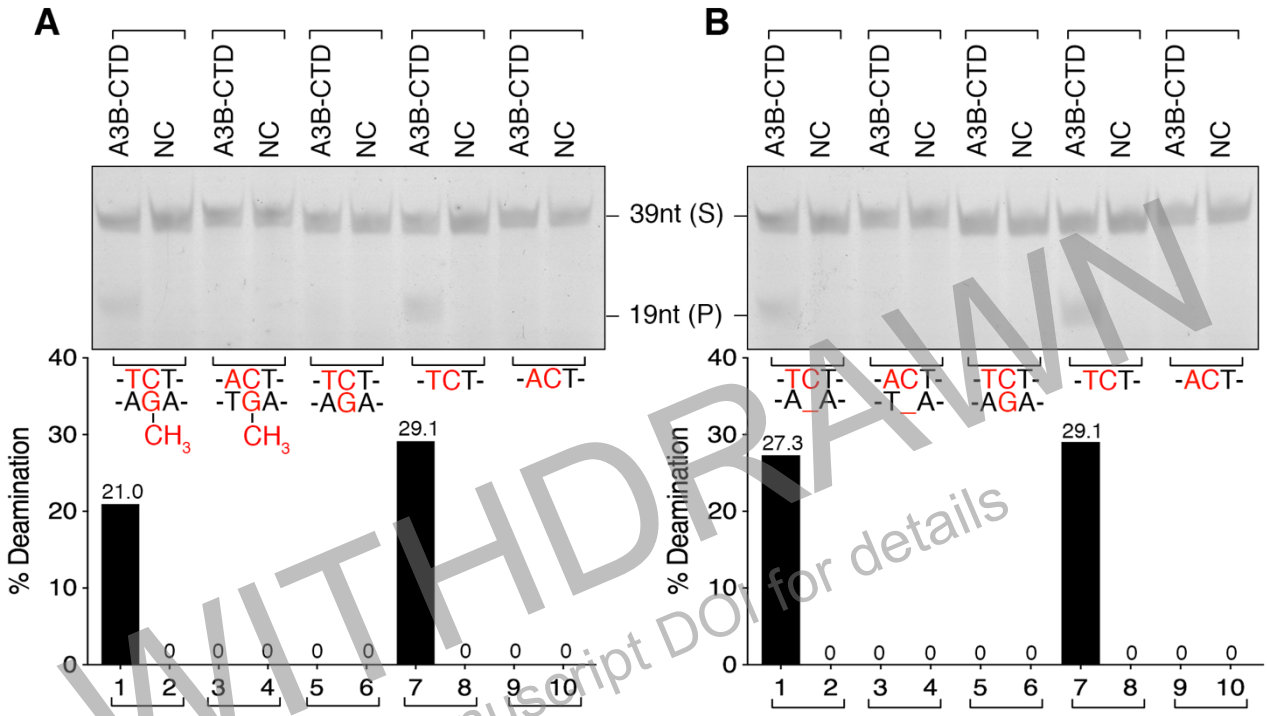

WITHDRAWN
see manuscript DOI for details

Fig. 3*: The A3B C-terminal domain (CTD) is sufficient to deaminate the dsDNA A3B substrates in vitro*. (A, B) *in vitro* deamination with purified A3B-CTD and NC (negative control, A3B-CTD buffer) on 39 bp oligonucleotides. Bar graphs indicate the amount of cleaved product relative to the amount of starting substrate. S, substrate; P, cleaved product.

bioRxiv preprint doi: https://doi.org/10.1101/750877; this version posted August 29, 2019. The copyright holder for this preprint (which was not certified by peer review) is the author/funder. All rights reserved. No reuse allowed without permission.

WITHDRAWN
see manuscript DOI for details

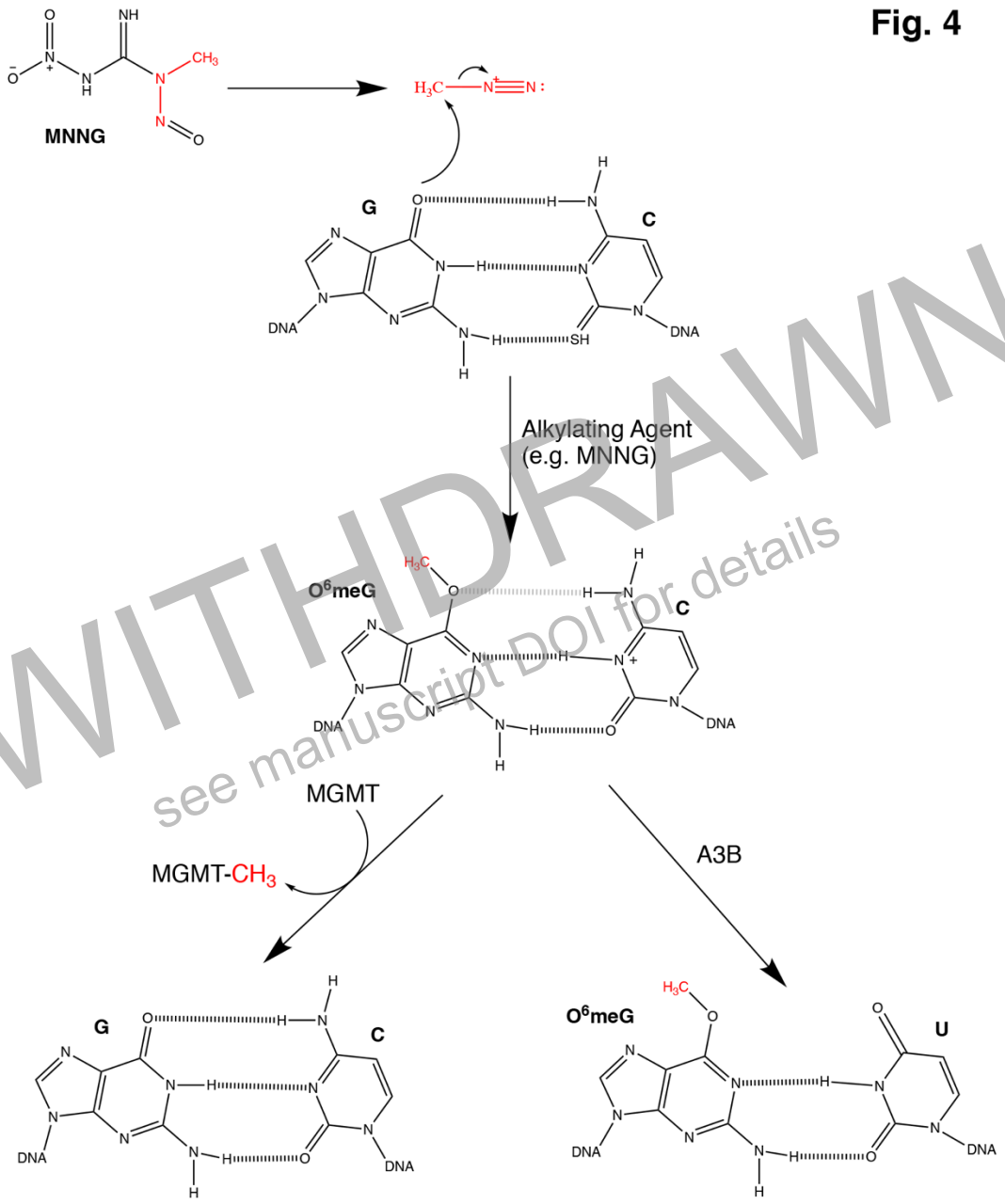

Fig. 4*: Proposed molecular model of MNNG-generated A3B substrate*. Electrons on O^6-G can attack the carbon of a methane diazonium cation (metabolic product of MNNG), resulting in the addition of an O^6-methyl group on guanine. The weakened O^6-G/N^4-C hydrogen bond (gray) allows A3B to deaminate C, resulting in an O^6meG/U base pair (right arrow). MGMT transfers the O^6-methyl to its active site cysteine (Cys145), restoring the G/C base pair and inactivating MGMT (left arrow).

bioRxiv preprint doi: https://doi.org/10.1101/750877; this version posted August 29, 2019. The copyright holder for this preprint (which was not certified by peer review) is the author/funder. All rights reserved. No reuse allowed without permission.

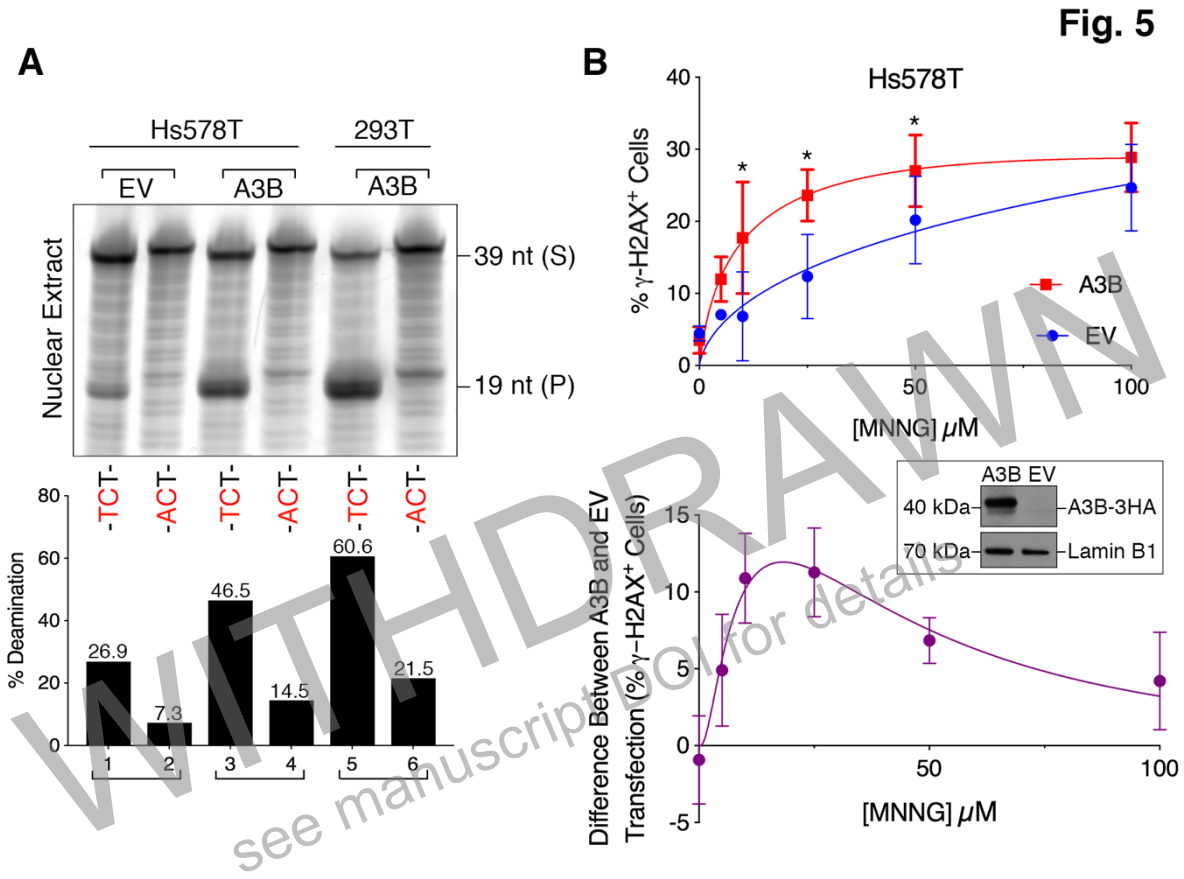

WITHDRAWN
see manuscript DOI for details

Fig. 5*: A3B enhances MNNG-induced γ-H2AX foci in Hs578T cells.* (A) *in vitro* deamination on 39 bp oligonucleotides (containing TC or AC motifs) using Hs578T nuclear extracts transfected with the A3B-HA or EV expression vector. Bar graph shows the amount of cleaved product relative to the amount of starting substrate. (B) Insert shows western blot of Hs578T cells transfected with A3B-HA or empty expression vectors probed with anti α-HA, or α-LaminB1 (loading control). Upper panel shows the effect of A3B expression on γ-H2AX foci (red) induced by various concentrations of MNNG compared to empty vector (blue). A3B expression alone does not produce detectable γ-H2AX foci at 0 μM MNNG, using the fluorescence threshold set for these experiments (see MATERIALS AND METHODS). n = 30 fields of view per sample from 3 independent trials, error bars represent standard deviation. Paired, two-tailed student's t-tests confirm statistical significance (*, $p < 0.05$) at 10, 25 and 50 μM MNNG. Bottom panel shows the difference between the γ-H2AX foci detected in cells transfected with the A3B (red) or EV (blue) expression vectors, error bars represent standard deviation.

bioRxiv preprint doi: https://doi.org/10.1101/750877; this version posted August 29, 2019. The copyright holder for this preprint (which was not certified by peer review) is the author/funder. All rights reserved. No reuse allowed without permission.

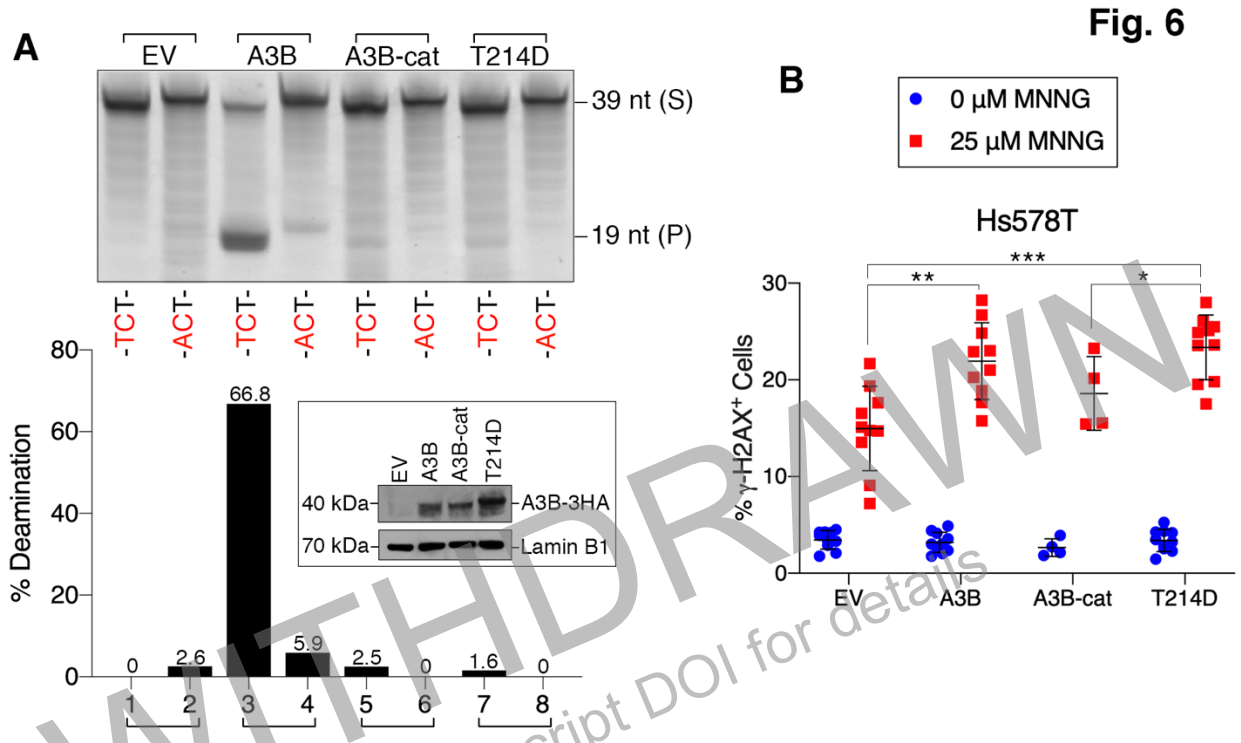

WITHDRAWN
see manuscript DOI for details

Fig. 6: *Effect of A3B deaminase activity on MNNG-induced γ-H2AX foci.* (A) *in vitro* deaminase activity of extracts of Hs578T cells transfected with the indicated expression vectors. Bar graph represents the amount of cleaved product produced by A3B deamination relative to the amount of starting substrate. Insert shows a western blot of the levels of A3B protein generated by the various expression vectors in Hs578T cells probed with anti α-HA, or α-LaminB1 as a loading control. S, substrate; P, cleaved product. (B) γ-H2AX foci in Hs578T cells that had been transfected with the indicated A3B expression vectors then treated with 25 μM MNNG (1 h) followed by a 1 h recovery as described in MATERIALS AND METHODS. EV, empty vector; A3B-cat, double deaminase mutant. n = 4 (A3B-cat), n = 10 (EV, A3B, T214D), line represents mean, error bars represent standard deviation. Two-tailed t-tests (equal variance) confirm statistical significance (*, **, ***; $p < 0.05, 0.01, 0.001$ respectively).

bioRxiv preprint doi: https://doi.org/10.1101/750877; this version posted August 29, 2019. The copyright holder for this preprint (which was not certified by peer review) is the author/funder. All rights reserved. No reuse allowed without permission.

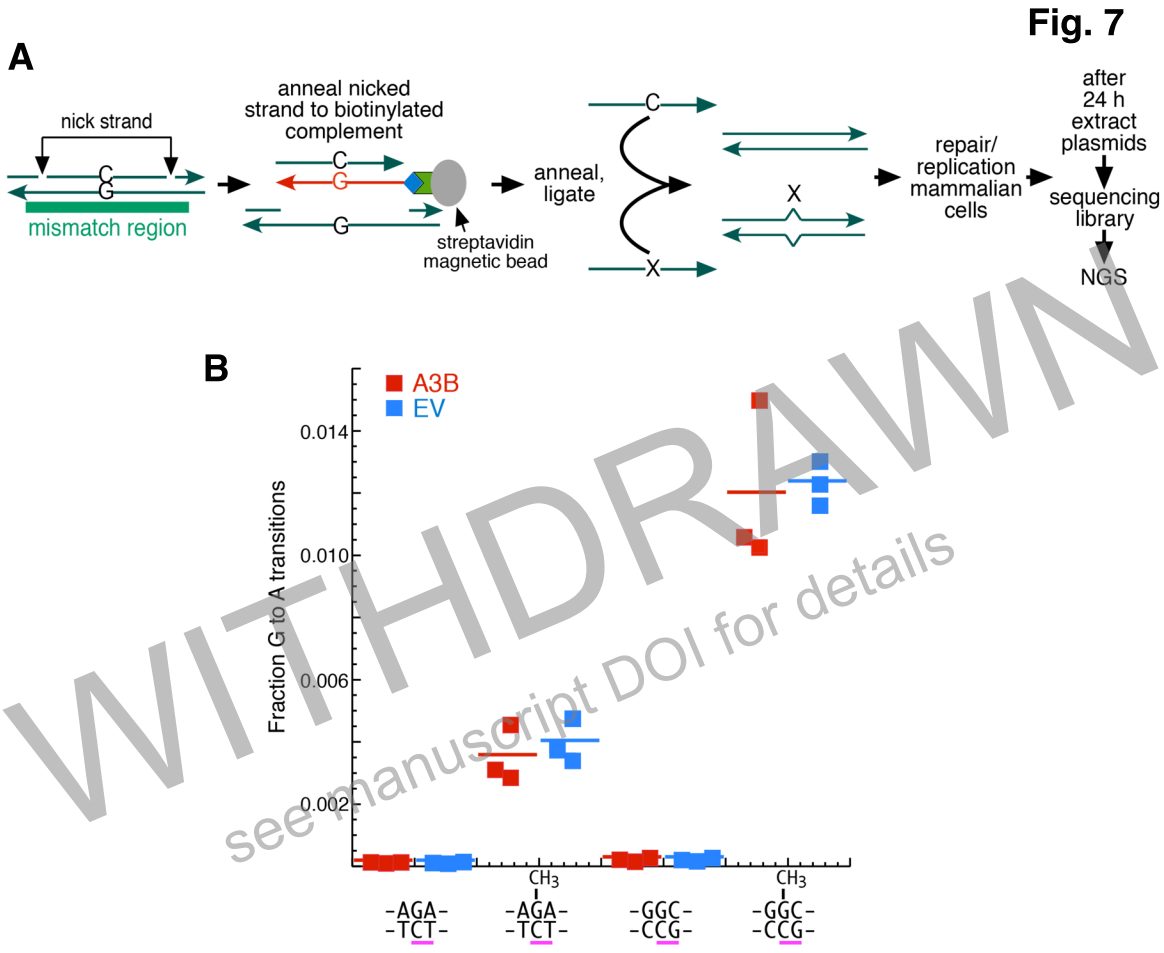

WITHDRAWN
see manuscript DOI for details

Fig. 7: *Fate of O⁶meG/C base pair on a shuttle vector in breast cancer cells.* (A) Schematic of mismatch plasmid construction. See MATERIALS AND METHODS for details. (B) The recovery of G to A transitions of O⁶meG paired to C in a TC context occurs one third as often compared to when the C is in a GC context. Horizontal line represents mean. In both cases >99.9% of G transitioned to A (Supplementary Table **S4**).